Published in final edited form as:
Nat Chem. 2011 March ; 3(3): 249–255. doi:10.1038/nchem.961.

Single cells and intracellular processes studied by a plasmonic-based electrochemical impedance microscopy

Wei Wang, **Kyle Foley**, **Xiaonan Shan**, **Shaopeng Wang**, **Seron Eaton**, **Vinay J Nagaraj**, **Peter Wiktor**, **Urmez Patel**, and **Nongjian Tao***
Center for Bioelectronics and Biosensors, Biodesign Institute, Department of Electrical Engineering, Arizona State University, Tempe, AZ 85287

Abstract

We report an electrochemical impedance microscope (EIM) based on surface plasmon resonance. The new EIM can resolve local impedance with sub-micron spatial resolution, and monitor dynamics of various processes, such as apoptosis and electroporation of individual cells with millisecond time resolution. The high spatial and temporal resolution images make it possible to not only study individual cells, but also resolve the sub-cellular structures and processes without labels. The detection sensitivity achieved with the current setup is ~2 pS, which is excellent considering the conductance of a single ion channel is in the range of 5–400 pS. We describe also a model that simulates the EIM images of cells based on local dielectric constant and conductivity.

Continued advances in science depend critically on the development of new enabling spectroscopic and microscopic tools. One important example is Electrochemical Impedance Spectroscopy (EIS). This label free technique has been developed to study and detect various biological substances, from DNA and proteins to viruses and bacteria[1,2]. Giaever et al.[3,4] has pioneered an EIS method to study many cellular processes, including cell spreading, adhesion, invasion, toxicology and motility. Although powerful, conventional EIS lacks spatial information, which is essential for studying heterogeneous processes and for imaging high-throughput microarrays. A particularly important example is the recent trend of studying cellular heterogeneity, which demands new tools for single cell analysis[5,6]. We show here an electrochemical impedance microscope (EIM) that can resolve local impedance with sub-micron spatial resolution, and monitor various processes, such as apoptosis and electroporation of cells with millisecond time resolution. The high spatial and temporal resolution images make it possible to not only study individual cells, but also resolve the sub-cellular structures and processes without labels. Unlike conventional EIS that measures electrochemical current, the EIM is based on sensitive dependence of surface plasmon resonance (SPR) on surface charge density, which is measured optically, thus allowing for fast and non-invasive imaging of impedance. The EIM maps the local electrical polarizability and conductivity, which reflects local changes in the cellular structure and ionic distribution. This important information is not available by other microscopes.

The basic working principle of EIS is to apply an AC voltage (ΔV) to an electrode and monitor the current response (ΔI). The impedance, Z, determined by $Z=\Delta V/\Delta I$, is sensitive

*Corresponding authors: njtao@asu.edu.

Author contributions

KF performed initial impedance imaging of cells, WW carried out the measurement and data analysis presented here, XS contributed to the numerical simulation and prepared gold chips, SE, VJN and PW helped with the cell culture, KF and UP developed imaging processing software, WW, KF and SW designed and set up the experiment, NJT conceived the experiment and model simulation, and wrote the paper.

to processes, such as a molecular binding event and apoptosis of cells taking place on the electrode surface. To obtain spatial information, one could, in principle, use an array of microelectrodes[7–9]; each provides an impedance signal at a particular location. However, high spatial resolution requires a high-density array of microelectrodes, which demands sophisticated microfabrication, and complex interconnection and multiplexing of the microelectrodes.[10] Because of the electrochemical current scales with the size of the microelectrode, increasing spatial resolution by shrinking the microelectrodes will result in a decreasing impedance signal measured by each microelectrode, and the measurement is susceptible to unwanted electronic interference between closely spaced microelectrodes. For these reasons, high-resolution impedance microscopy using microelectrodes is not yet possible. An alternative approach is to measure the AC impedance between a microelectrode and a surface by mechanically scanning the microelectrode across the sample.[11,12] The measured impedance depends not only on the sample properties but also the impedance of the microelectrode, which complicates the interpretation of the data[13]. Furthermore, the mechanically scanning tip is slow and may introduce perturbation to the measurement. In the present work, the impedance is determined optically without microelectrodes, which overcomes the difficulties of the conventional impedance measurement, and in the mean time, allows for simultaneous optical and SPR imaging of the same sample, providing additional and complementary information.

The EIM relies on detecting surface plasmon waves propagating on a metal thin film (Fig. 1a). The surface plasmon waves are created with a laser beam incident on the metal film via, typically, a prism at a so-called resonant angle, and the reflected beam creates an SPR image. The resonant angle is sensitive to changes in refractive index near the metal surface, which has been widely used to study molecular binding processes,[14,15] and, more recently, to image electrochemical current.[16] In contrast, the EIM is based on the sensitive dependence of SPR on surface charge density. Like the conventional EIS, we apply an AC voltage to the surface to create a surface charge density modulation (Δq), which induces a SPR signal change ($\Delta\theta$). We have shown that the charge density is related to the SPR signal by $\Delta q(x, y, \omega) = \alpha\Delta\theta(x, y, \omega)$, where ω is the angular frequency of the AC modulation, and $\alpha \sim 28$ C m^{-2} deg^{-1} is a constant that can be determined either by experimental calibration or calculation[17]. From the surface charge density distribution, we determine local impedance by $Z^{-1}(x, y, \omega) = (j\omega\alpha)\Delta\theta(x, y, \omega)/\Delta V$, where ΔV is the amplitude of the AC modulation.

Our previous work[17] used a conventional SPR setup to demonstrate the possibility of measuring surface charge of a bare gold and self-assemble monolayer with static SPR, and the finding was modeled in terms of capacitors and resistors. However, since SPR probes only ~200 nm near the surface, and the capacitor-resistor model was inadequate to describe a heterogeneous sample, whether the concept can be applied to thick and heterogeneous samples, such as cells, was questionable. Besides, the spatial resolution of the conventional prism SPR setup was insufficient to resolve single cells. In the present work we develop a new impedance imaging capability with sub-micron spatial resolution, and signal-processing algorithm for fast video analysis, which make it possible to image single cells. More importantly, we show that the impedance-imaging concept works for thick and heterogeneous samples, and developed a microscopic model based on local electrical polarizability and conductivity, which not only validates the concept, but also provides a foundation for future impedance imaging of heterogeneous samples. Finally, we demonstrate for the first time that the new imaging technique can indeed be applied to image and study sub-cellular processes, apoptosis and electroporation.

Results and Discussion

Single cell detachment and numerical simulation

Fig. 2 shows simultaneously recorded optical, SPR and EIM images of a cultured human cervical cancer cell from the SiHa cell line undergoing early apoptosis. Note that the EIM image contrast is proportional to the inverse of the impedance (admittance). It demonstrates that EIM can resolve not only individual cells but also sub-cellular structures. For example, the nucleolus of the cell is shown as a dark spot in the EIM image (marked by a black arrow). Conventional EIS measures averaged impedance response over many cells on an electrode, which was modeled using a combination of resistors and capacitors, and the data are often expressed graphically a Bode or Nyquist plot.[18,19] The model treats cells as cylindrical disks described by a few simple parameters, which is useful for the interpretation of the EIS data, but not suitable for the present EIM that resolves internal structure of the each cell, and thus requiring a microscopic model. Since impedance measures the response of the cells to a small external electrical field, which can be modeled by local polarizability and conductivity (σ) of the cell and surrounding environment. Polarizability, quantified by the local dielectric constant (ε_r), describes the non-conductive regions, e.g., membranes, and the conductivity describes the ionic conduction. In a given region, both contributions may co-exist, which is described by a complex permittivity, $\varepsilon = \varepsilon_0\varepsilon_r + j\sigma/\omega$, where ε_0 is the vacuum permittivity. The real and imaginary parts of the permittivity correspond to the capacitive and resistive components in the conventional impedance models. The EIM image maps the local variations in the dielectric and conductive properties, which reflect changes in the cellular structure and ionic distribution. Such information is important for a better understanding of various cellular processes, but not available from the existing microscopes.

To further illustrate that local variation in the local polarizability and conductivity leads to an EIM image contrast, we have simulated the EIM of a cell attached to the surface numerically. The simulation includes a bottom electrode on which a cell is attached, a buffer medium and a top electrode. A voltage between the top and bottom electrodes provides a weak electric field and the local SPR response of the bottom electrode leads to an EIM image. The model cell contains cell membrane, cytoplasm and a nucleus and its envelope (Fig. 2d; see Supporting Information for more details). Although this model is simplified, it contains more structural details than the existing EIS models of cells, and can be expanded to include more details when needed. Fig. 2e shows a simulated EIM image, which captures the variations in the dielectric constant and conductivity in the cell. For comparison, a simulated SPR image based on the same model is shown in Fig. 2f.

Although the main goal of the present work is to demonstrate real-time imaging of single cells with the EIM, we have explored the capability of the new microscopy for monitoring cellular processes. Among the various cellular processes, the study of apoptosis, a programmed cell death process, is of paramount importance due its critical role in homeostasis, tissue/organ development and diseases such as cancer. The loss of mechanisms that regulate apoptosis leads to cancer and strategies for cancer therapy frequently rely on induction of apoptosis in malignant cells[20]. The induction and progression of cellular apoptotic events in the human papilloma virus 16 infected cervical cell line SiHa was investigated after treating the cells with tumor necrosis factor-related apoptosis-inducing ligand (TRAIL) in combination with the proteosome inhibitor MG132[21].

The simultaneously recorded optical, SPR, and EIM images provide rich and complementary information about the cellular processes during apoptosis. The conventional bright field optical image is well established, which serves as a reference technique. The SPR image resolves the bottom portion (~200 nm) of the cell on the surface, which is particularly useful for studying cell-surface interactions. As shown in Figs. 2b1–b3 the

apoptosis starts with a decrease in the SPR image brightness near the center of the cell, reflecting the detachment of the cell from the surface starting from the center. This detachment process is not resolved by the conventional optical image (Figs. 2a1–a3). The simultaneous EIM images (Figs. 2c1–c3) show large and dynamic changes of the cell during the apoptosis. For example, the nucleolus region changes rapidly in the EIM images (but not in the conventional optical image). Previously the investigation of such changes to the nucleolus has been possible only through fluorescent staining or by using electron microscopy. The region pointed by a black arrow shows a large increase in the image intensity, which is not resolved by either the optical image or the SPR image. Based on the model described above, we have simulated both SPR (insets in Figs. 2b1–b3) and EIM images (insets in Figs. 2c1–c3) during apoptosis. The simulated SPR image reproduces the observed decrease in brightness starting from the cell center (see Supporting Information). The simulated EIM image reproduces the basic features of the measured image, including the decrease in the contrast of the nucleolus.

Apoptosis

A better way to view the wealthy information of EIM is via video. Fig. 3 shows a sequence of snapshots of both SPR (Fig. 3a) and EIM (Fig. 3b) videos of two cells during apoptosis (see Supporting Information for the videos). For comparison, the conventional optical images of the cells recorded in the beginning (Fig. 3c) and last stages (Fig. 3h) of the apoptosis are also shown. By selecting different regions of the images, quantitative local and total impedance information vs. time can be readily obtained. For example, by selecting the entire region of each cell, the total impedance responses of the two cells as a function of time can be analyzed (Fig. 3f). Although the impedance responses of both cells decrease with time, they occur at different rates, reflecting heterogeneity of cell apoptosis, which underscores the importance of single cell analysis. The decreases in the total impedance responses of the two cells are mainly due to the detachment of the cells from the electrode surface, which is evident from the SPR and optical images. In fact, the total SPR image intensities of the two cells vs. time show a similar behavior (Fig. 3d).

By selecting different regions within a cell, one can also follow the impedance change of a particular region of interest. Fig. 3g plots the impedance responses of the nucleus region and an adjacent region of the cell 1. The response of the nucleus region of cell 1 (marked by R1 in Fig. 3c) increases initially and then decreases after reaching a peak. This is in contrast to that of the adjacent region (marked by R2 in Fig. 3c), which decreases monotonically. The corresponding time-profiles of the two selected regions of the SPR images are plotted in Fig. 3e, showing also different responses of the two regions. For region 2, the SPR signal decreases smoothly, which is comparable to the EIM response. In contrast, for region 1, the SPR signal drops suddenly when the EIM response reaches the maximum. The different responses of cells 1 and 2, and local regions R1 and R2 within cell 1 are due to heterogeneous cellular apoptosis processes, which have be resolved by the EIM.

Electroporation

We have also applied the EIM to study electroporation, a process that has been used for introducing DNA and drugs into cells.[22,23] Electroporation can be trigged by applying a voltage pulse to a cell, which create large increases in the electrical conductivity and permeability of the cell plasma membranes.[24] We have recorded EIM images (together with optical and SPR images) of electroporation processes. Fig. 4 shows a sequence of snapshots of an electroporation process, and a complete video of the process is available in the Supporting Information. The optical image shows little changes during and after the electroporation process, as shown in Figs. 4c and 4h, respectively. The SPR image shows a large change during the process. For example the regions marked by red arrows in Fig. 4a

show relatively large decrease in the brightness when electroporation potential was applied for 3 seconds, indicating local detachment of the cell membrane from the surface. However, the SPR image recovers after the large transient change within a minute. The EIM image shows the most dramatic changes. It starts with a large and rapid increase in the impedance response, and then followed by a recovery process much slower than the SPR image.

The time-profiles of selected regions show more clearly the changes in the SPR and impedance images. The SPR profile of the cellular region (red and green in Fig. 4d) shows a large negative response, which recovers over ~ 60 sec. Note that the SPR signal recovery is complete, which is similar to the conventional optical images (Figs. 4c and 4h). The time-profiles of the corresponding regions for the EIM are shown in Figs. 4f and 4g. In sharp contrast to the SPR and optical images, the impedance signal of the cellular region shows a large increase and then followed by a slow decay. The large change in the impedance signal is expected during the electroporation that creates openings in the cell membranes. The change is not uniform across the entire cell. For example, the SPR and impedance signals from two selected regions, marked by R1 and R2 are shown in Fig. 4c. It is clear that both the SPR and impedance responses for region 1 are much larger than those of region 2. Unlike the optical and SPR images, the impedance signal of the cell does not fully recover its initial value. We believe that the residual change is due to a slow recovery process because the complete electroporation healing of cells attached on gold surface usually takes several hours according to a previous report[24].

Spatial resolution of the EIM along the direction of surface plasmon waves is determined by the plasmon propagation distance, which depends on the electrode material and wavelength of incident light. For a gold electrode in aqueous solutions, the spatial resolution along the plasmon waves is ~3 μm using 635 nm light. Fig. 1b shows the impedance image of a 200 nm silica nanoparticle. However, if using 532 nm light, the resolution improves to ~0.2 μm. Perpendicular to the plasmon propagation direction, the resolution is determined by the diffraction limit. Using a numerical aperture of 1.65, the diffraction limit is about ~0.2 μm. The detection limit of the local impedance depends also on several factors, including the amplitude and frequency of applied voltage modulation, light source, camera, and thermal and mechanical noises. In the present system, the detection limit in terms of admittance (inverse of impedance) is about ~2 pS (assuming modulation amplitude=0.1 V, modulation frequency=170 Hz, wavelength of light=635 nm), which is excellent considering the conductance of a single ion channel is between 5–400 ps. The frequency range of the EIM is determined by the camera speed, which has a maximum frame rate of 380 frames per second in our setup. In the present work we image cells as a function of time at fixed frequencies. Fast CCD with a frame rate of MHz is available which can speed up the EIM for detecting extremely fast event. This will also make it possible to acquire EIM images by scanning the frequency over a wide range to obtain additional information. Finally we point out that unlike fluorescence imaging, the temporal resolution of SPR based EIM imaging is not limited by the light emitting intensity.

We have demonstrated an EIM that images structural and ionic distribution changes in individual adherent cultured mammalian cells. The EIM is label-free, non-invasive and has high spatial and temporal resolutions, which provides local impedance information that is not available before. Further systematic studies will help to develop a microscopic model that relates various cellular processes to local conductivity and dielectric responses, and interpret the data obtained with widely used EIS measurements of cells. We also anticipate that the new EIM to have broad application in research involving drug discovery for cancer therapy and other diseases, host cell-pathogen interactions, differentiation of stem cells, as well as studies involving label-free biomolecular interactions of DNA, proteins, enzymes, sugars, lipids etc. using microarrays.

Methods

Cell culture

The human cervical cell line SiHa was purchased from the American Type Culture Collection (Manassas, VA). SiHa cells were cultured in a humidified atmosphere at 37 °C with 5% CO_2 and 70% relative humidity. Cells were grown in Dubelco's modified eagle's medium (DMEM; Invitrogen, Carlsbad, CA) with 10% fetal bovine serum (FBS; Invitrogen, Carlsbad, CA) with penicillin and streptomycin (BioWhittaker, Basel, Switzerland). Cells were passaged with 0.05% Trypsin and 0.02% ethylenediamine-tetraacetic acid (EDTA) in Hank's balanced salt solution (HBSS; Sigma-Aldrich, St. Louis, MO) when they reached a confluency of approximately 75%.

Impedance measurements

The imaging setup was based an objective-based inverted microscope system introduced by Zare et al.[25] The optical system comprises a He-Ne laser source (633 nm), an optical fiber, an inverted microscope (Olympus X81) and a charge-coupled device (CCD) camera (Pike F-032). The sensor chip was a BK7 glass coverslip coated with ~2 nm of chromium followed by ~47 nm of gold. Each chip was washed by water and ethanol followed by hydrogen flame annealing to remove surface contamination prior to use. A Flexi-Perm silicon chamber (Greiner Bio-One) was placed on top of the gold chip and acted as both cell culture well and electrochemical cell. The potential of the sensor surface was controlled with respect to a silver wire quasi-reference electrode with a bipotentiostat (Pine ARFDE5) and platinum wire counter electrode. The modulation with frequency 170 Hz and amplitude up to 150 mV was applied via an external function generator. We also applied lower amplitude modulation which produced more noisy but similar images for the samples studied in this work (surface covered with a layer of molecules).

To seed SiHa cells on the gold chip, 200 μL of growth medium with 5,000 cells was added a FlexiPerm well attached to the chip. The seeded chips were placed in an enclosed culture chamber (Tokaihit INU-ONICS-F1) on the microscope platform with controlled conditions (37 °C temperature, 5% CO_2 and 75% relative humidity). After overnight incubation, the cells adhered to the gold surface and spread out. Controlled conditions were maintained through the experiment.

Apoptosis and electroporation

To induce the apoptosis, 10 μM proteosome inhibitor MG132 (Sigma) was added and incubated for two hours and then 1 μg/ml of human recombinant TRAIL (Calbiochem/EMD Biochemicals, Gibbstown, NJ) consisting of the amino acid sequence from 114–281 was added before EIM measurements. For electroporation, 1MHz AC modulation with a 20V Vpp was applied on the electrode and the duration time was 3 seconds.

Video processing

Postprocessing of data was accomplished using a program written in Matlab. A 25 points 2-D finite impulse response filter was applied to each image in order to minimize the intensity fluctuation for a single pixel. Sampling time was 2 seconds for fast Fourier transform (FFT) process. Typically, when the camera frame rate was 380 frames/s, 760 filtered images were processed pixel-by-pixel by FFT to create an amplitude image and an averaged SPR image. SPR video and EIM video were constructed from a series of averaged SPR images and amplitude images at different time, respectively.

EIM and SPR Image modeling

The EIM was modeled using COMSOL, a multiphysics modeling and simulation package that solves the Maxwell equations with proper boundary conditions. The cell was modeled as a hemispherical shaped structure attached to the gold electrode. The model cell included a membrane, a cytoplasm medium, a nucleus and its envelope, each with a different dielectric constant and conductivity (ε= 6.2, 60, 28, and 52; σ=0.169, 0.5, 0.01, and 1.35 $S \cdot m^{-1}$ for the membrane, cytoplasm, nucleus envelope and nucleus, respectively). The simulation also assumed that the buffer medium had dielectric constant and conductivity of 79 and 1.69 $S \cdot m^{-1}$, respectively. Solving the Maxwell equations numerically, we obtained the electric field near the bottom electrode, from which the local surface charge density modulation (Δq) was obtained. The EIM image was obtained based on $Z^{-1}=j\omega\Delta q/\Delta V$. The SPR simulation was carried out by $n(x,y,z)e^{-z/l}$, where n(x,y,z) is the local refractive index of the cell and surrounding medium, and exponential term reflects the decay of the evanescent field (decay length, l~200 nm).

Supplementary Material

Refer to Web version on PubMed Central for supplementary material.

Acknowledgments

We thank NIH (R21RR026235) and NSF (CHE-0554786) for support.

References

1. Katz E, Willner I. Probing Biomolecular Interactions at Conductive and Semiconductive Surfaces by Impedance Spectroscopy: Routes to Impedimetric Immunosensors, DNA-Sensors, and Enzyme Biosensors. Electroanal. 2003; 15:913–947.
2. Maalouf R, et al. Label-free detection of bacteria by electrochemical impedance spectroscopy: Comparison to surface plasmon resonance. Anal. Chem. 2007; 79:4879–4886. [PubMed: 17523594]
3. Giaever I, Keese CR. A morphological biosensor for mammalian-cells. Nature. 1993; 366:591–592. [PubMed: 8255299]
4. Giaever I, Keese CR. Monitoring Fibroblast behavior in tissue-culture with an applied electric field. Proceedings of the National Academy of Sciences USA. 1984; 81:3761–3764.
5. Slack MD, Martinez ED, Wu LF, Altschuler SJ. Characterizing heterogeneous cellular responses to perturbations. Proc. Natl. Acad. Sci. USA. 2008; 105:19306–19311. [PubMed: 19052231]
6. Schulte A, Schuhmann W. Single-cell microelectrochemistry. Angew. Chem. Int. Ed. 2007; 46:8760–8777.
7. Rothermel A, et al. Real-time measurement of PMA-induced cellular alterations by microelectrode array-based impedance spectroscopy. BioTechniques. 2006; 41:445–450. [PubMed: 17068960]
8. Rahman ARA, Register J, Vuppala G, Bhansali S. Cell culture monitoring by impedance mapping using a multielectrode scanning impedance spectroscopy system (CellMap). Physio. Meas. 2008; 29:S227–S239.
9. Chai KTC, Davies JH, Cumming DRS. Electrical impedance tomography for sensing with integrated microelectrodes on a CMOS microchip. Sens. Actuat. B. 2007; 127:97–101.
10. Lin Z, Ino K, Shiku H, Matsue T. Electrochemical topography of a cell monolayer with an addressable microelectrode array. Chem. Communications. 2010; 46:559–561.
11. Alpuche-Aviles MA, Wipf DO. Impedance Feedback Control for Scanning Electrochemical Microscopy. Anal. Chem. 2001; 73:4873–4881. [PubMed: 11681463]
12. Katemann BB, Schulte A, Calvo EJ, Koudelka-Hep M, Schuhmann W. Localised electrochemical impedance spectroscopy with high lateral resolution by means of alternating current scanning electrochemical microscopy. Electrochemistry Communications. 2002; 4:134–138.

13. Ervin EN, White HS, Baker LA. Alternating current impedance imaging of membrane pores using scanning electrochemical microscopy. Anal. Chem. 2005; 77:5564–5569. [PubMed: 16131066]
14. Rothenhausler B, Knoll W. Surface-Plasmon Microscopy. Nature. 1988; 332:615–617.
15. Andersson O, Ulrich C, Bjorefors F, Liedberg B. Imaging SPR for detection of local electrochemical processes on patterned surfaces. Sens. Actuat. B. 2008; 134:545–550.
16. Shan XN, Patel U, Wang SP, Iglesias R, Tao NJ. Imaging Local Electrochemical Current via Surface Plasmon Resonance. Science. 2010; 327:1363–1366. [PubMed: 20223983]
17. Foley KJ, Shan X, Tao NJ. Surface impedance imaging technique. Anal. Chem. 2008; 80:5146–5151. [PubMed: 18484741]
18. Giaever I, Keese CR. Micromotion of mammalian-cells measured electrically. Proceedings of the National Academy of Sciences USA. 1991; 88:7896–7900.
19. Urdapilleta E, Bellotti M, Bonetto FJ. Impedance analysis of cultured cells: A mean-field electrical response model for electric cell-substrate impedance sensing technique. Phys. Rev. E. 2006; 74:041908.
20. Bremer E, van Dam G, Kroesen B, de Leij L, Helfrich W. Targeted induction of apoptosis for cancer therapy: current progress and prospects. Trends Mol Med. 2006; 12:382–393. [PubMed: 16798087]
21. Hougardy BMT, et al. Proteasome inhibitor MG132 sensitizes HPV-positive human cervical cancer cells to rhTRAIL-induced apoptosis. International Journal of Cancer. 2006; 118:1892–1900.
22. Aihara H, Miyazaki J-i. Gene transfer into muscle by electroporation in vivo. Nature Biotechnology. 1998; 16:867–870.
23. Olofsson J, et al. Single-cell electroporation. Current Opinion in Biotechnology. 2003; 14:29–34. [PubMed: 12565999]
24. Keese CR, Wegener J, Walker SR, Giaever I. Eletrical wound-healing assay for cells in vitro. Proc. Natl. Acad. Sci. USA. 2004; 101:1554–1559. [PubMed: 14747654]
25. Huang B, Yu F, Zare RN. Surface Plasmon Resonance Imaging Using a High Numerical Aperture Microscope Objective. Anal. Chem. 2007; 79:2979–2983. [PubMed: 17309232]

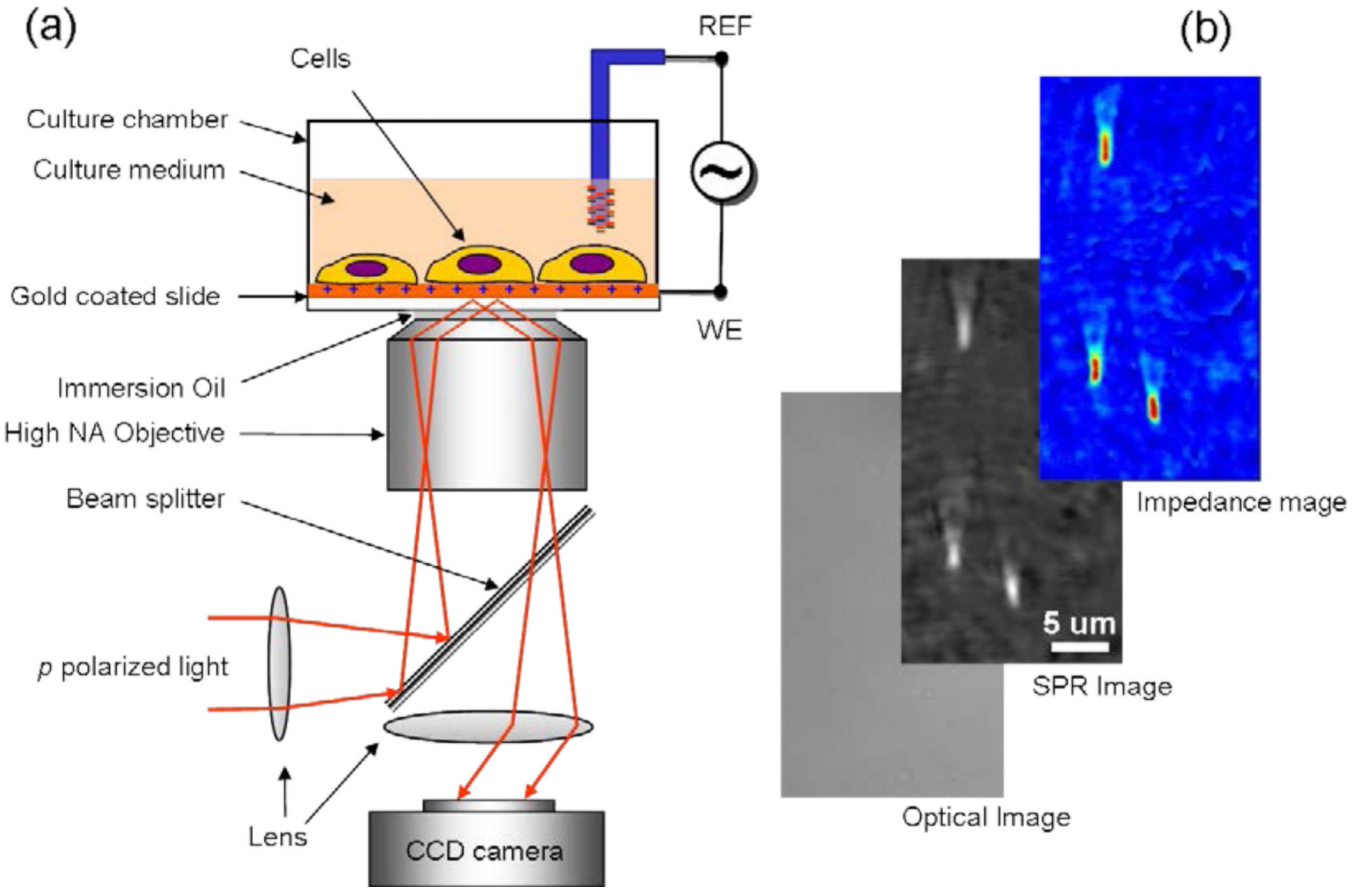

Figure 1. Electrical Impedance Microscopy

(a) Schematic illustration of the experimental setup. A laser beam is directed onto a gold-coated glass coverslip via an oil immersion objective to create surface plasmon resonance (SPR) on the gold surface, which is imaged with a CCD. On the coverslip cells are cultured for study. An AC modulation potential is applied to the gold electrode relative to a reference electrode inserted in the solution, and the impedance image (EIM) was created from the potential-induced SPR signal changes. In addition to the SPR and EIM images, a conventional optical image of the same sample is also available. (b) Example of optical, SPR and EIM images of 200 nm-silica nanoparticles to demonstrate spatial resolution. The optical image cannot resolve the nanoparticles, and the SPR image shows each nanoparticle as a bright spot with a long tail in the SPR propagation direction. The EIM image has similar spatial resolution as the SPR image.

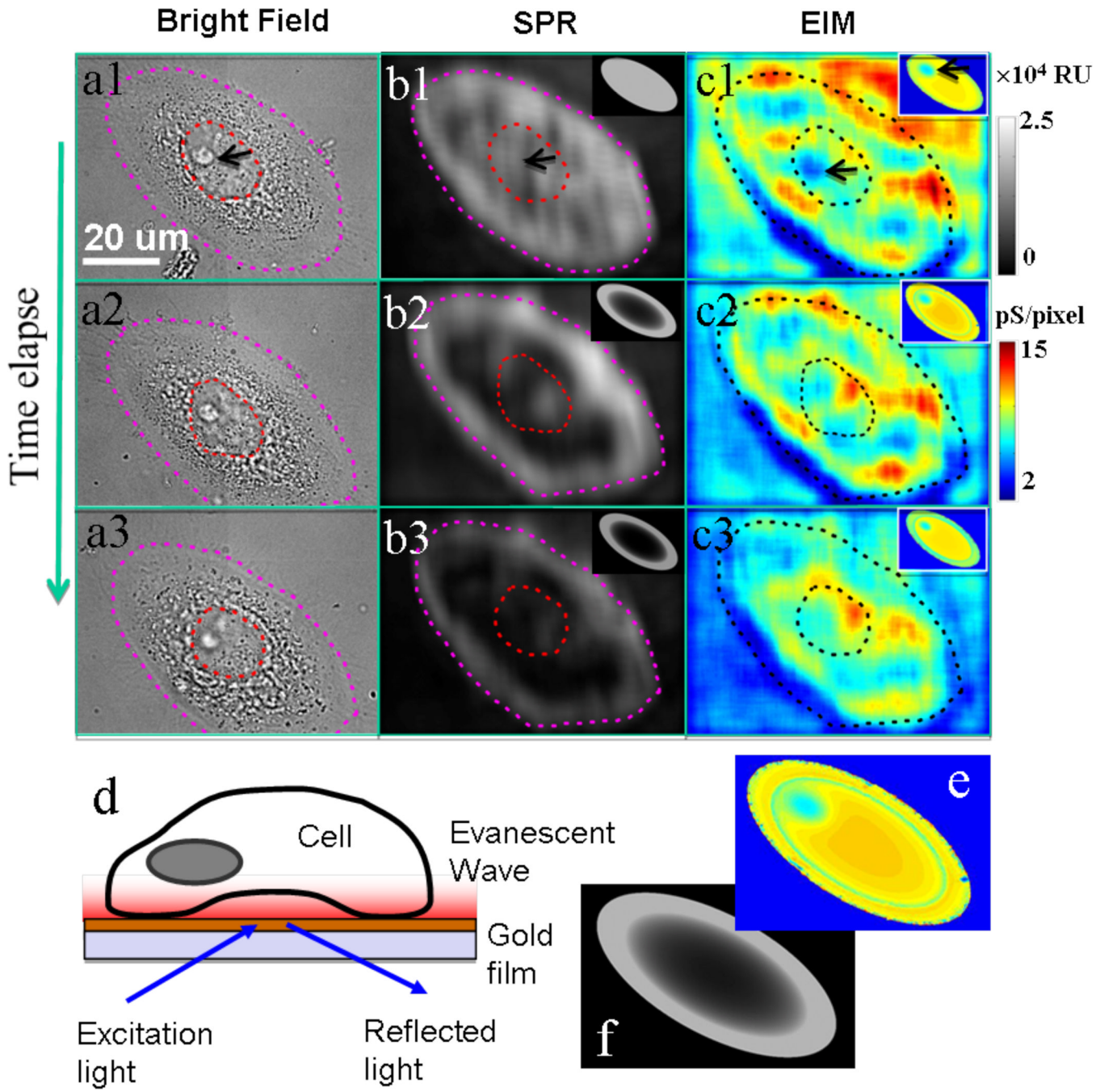

Figure 2. Impedance images of a single cell and model simulation

The simultaneously recorded optical transmission (a), SPR (b) and EIM (c) images of a SiHa cell at 0 (1), 30 (2) and 75 (3) min after apoptosis treatment. Schematic illustration of SPR imaging (d) showing that evanescent field localized near the surface interacts with the bottom portion of a cell. The evanescent wave here is an exponential-decaying wave at the glass-gold interface. Simulated EIM (f) and SPR (e) images that reproduce the main features observed in the experimental images. Note that the dashed circles outline the cell nucleus, and the black arrows point the nucleolus of the cell. Gray scale-bar is the z-axis scale of SPR with the unit of RU. Color scale-bar is the z-axis scale of EIM with the unit of pS/pixel. The size of a single pixel is about 0.0625 μm^2 (0.25μm × 0.25μm).

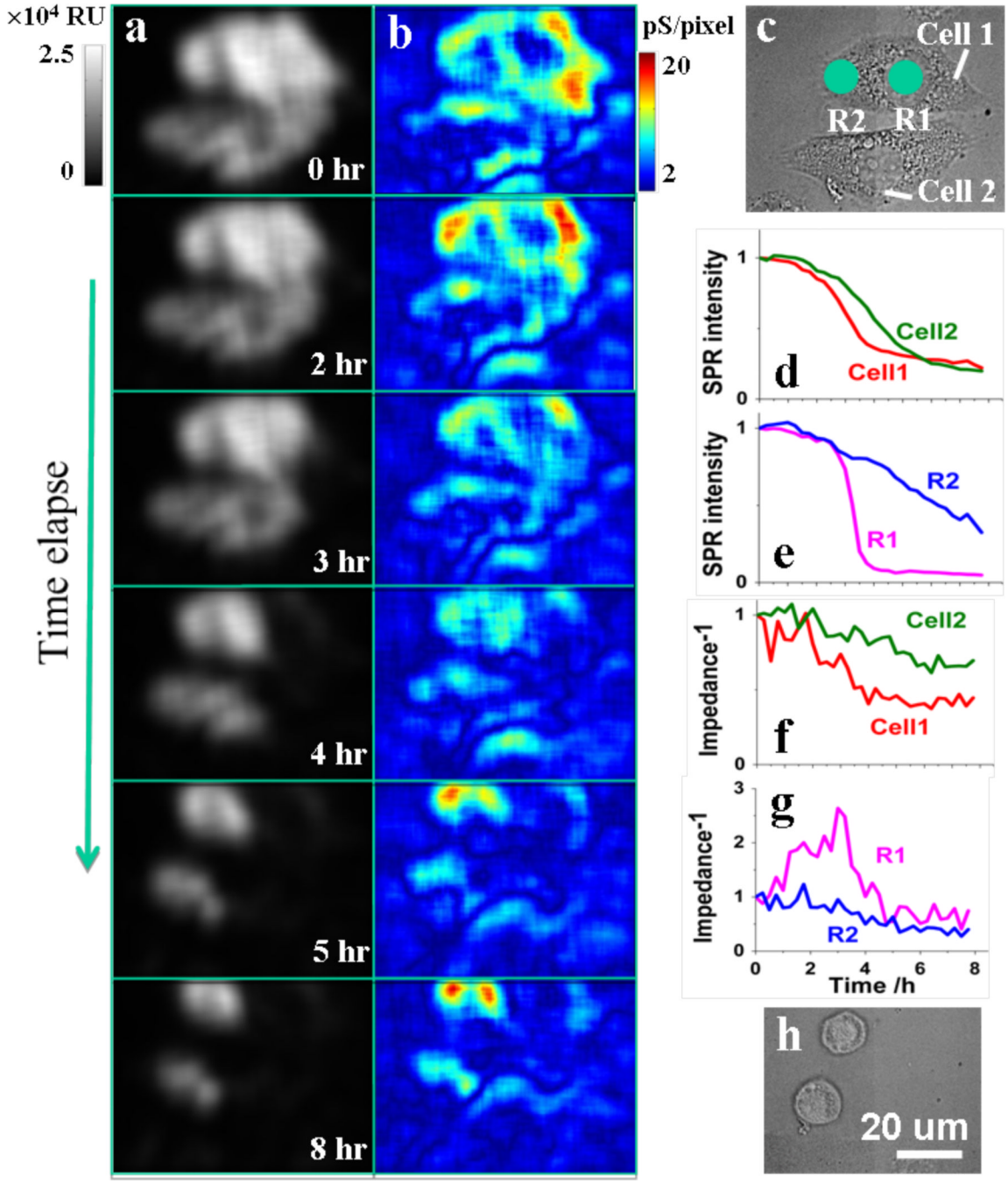

Figure 3. Monitoring single cell apoptosis with EIM

A sequence of snapshots of apoptotic events in SiHa cells illustrates the time-dependent SPR (a) and EIM images (b). Bright field optical images before (c) and after (h) apoptosis are presented to show the morphology change. Quantitative profiles of SPR (d, e) and EIM (f, g) are analyzed for individual cells (d, f) and sub-cellular regions (e, g) within a single cell. Gray scale-bar is the z-axis scale of SPR with the unit of RU. Color scale-bar is the z-axis scale of EIM with the unit of pS/pixel. The size of a single pixel is about 0.0625 μm^2 (0.25μm × 0.25μm).

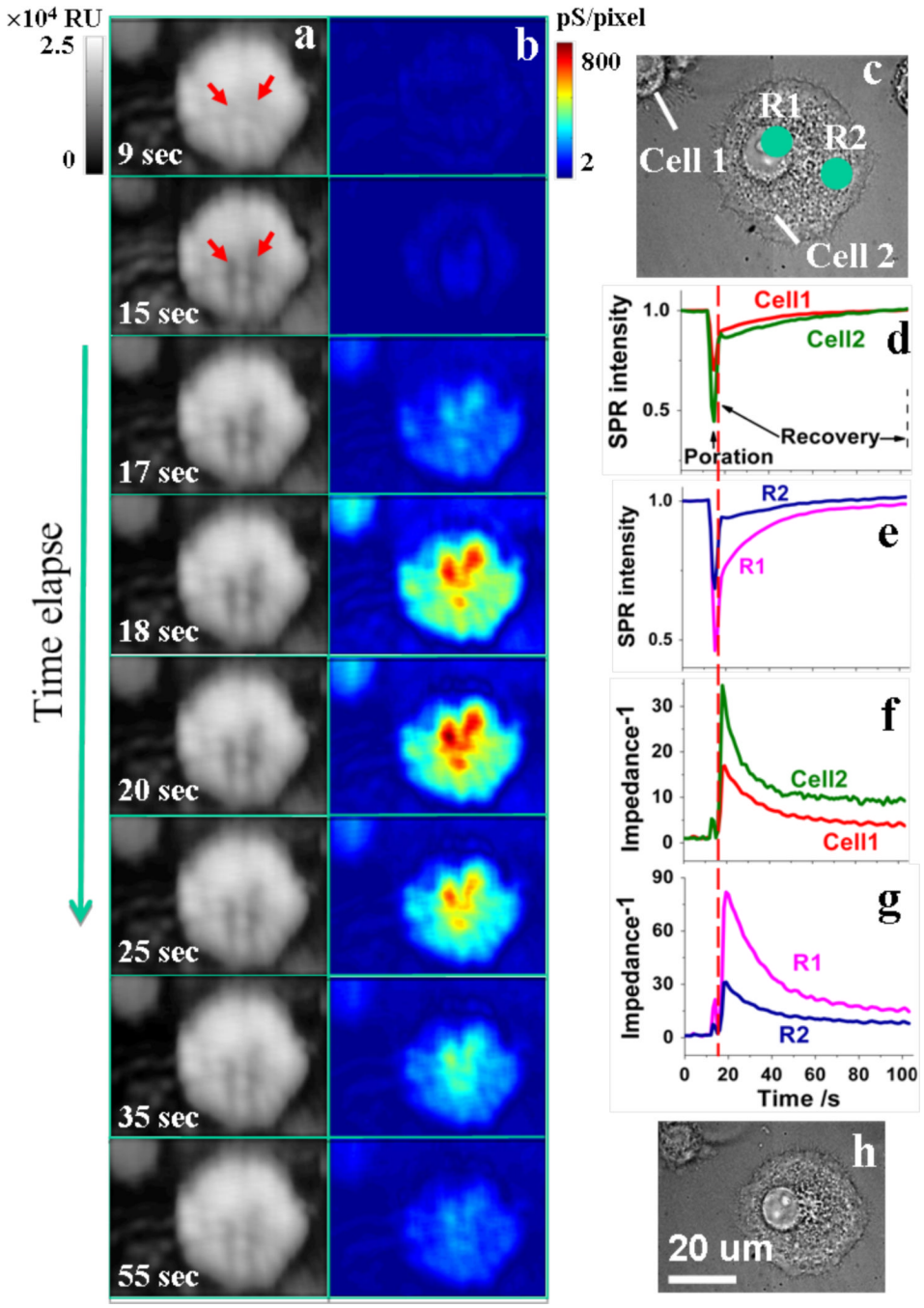

Figure 4. Monitoring single cell electroporation with EIM

Time-dependent SPR (a) and EIM images (b) during an electroporation process. Bright field optical images before (c) and after (h) electroporation are presented to show the morphology change. Quantitative profiles of SPR (d, e) and EIM (f, g) are analyzed for individual cells (d, f) and sub-cellular regions (e, g) within a single cell. R1 and R2 mark two regions within the cell. Gray scale-bar is the z-axis scale of SPR with the unit of RU. Color scale-bar is the z-axis scale of EIM with the unit of pS/pixel. The size of a single pixel is about 0.0625 μm^2 (0.25μm × 0.25μm).